

# Fully Proprioceptive Slip-Velocity-Aware State Estimation for Mobile Robots via Invariant Kalman Filtering and Disturbance Observer

Xihang Yu, Sangli Teng, Theodor Chakhachiro, Wenzhe Tong, Tingjun Li, Tzu-Yuan Lin  
Sarah Koehler, Manuel Ahumada, Jeffrey M. Walls, and Maani Ghaffari

**Abstract**—This paper develops a novel slip estimator using the invariant observer design theory and Disturbance Observer (DOB). The proposed state estimator for mobile robots is fully proprioceptive and combines data from an inertial measurement unit and body velocity within a Right Invariant Extended Kalman Filter (RI-EKF). By embedding the slip velocity into  $SE_3(3)$  Lie group, the developed DOB-based RI-EKF provides real-time accurate velocity and slip velocity estimates on different terrains. Experimental results using a Husky wheeled robot confirm the mathematical derivations and show better performance than a standard RI-EKF baseline. Open source software is available for download and reproducing the presented results.

## I. INTRODUCTION

For mobile robots, state estimation is the problem of determining a robot’s position, orientation, and velocity with respect to a fixed world or body frame [1]. This problem is vital for many robotics tasks such as control [2]–[4] or trajectory planning [5], [6]. The filtering approach takes low computational resources and often operates at a high frequency [7]–[10]. One interesting class of estimators is the Invariant Extended Kalman Filter (InEKF). Matrix Lie groups provide natural (exponential) coordinates that exploits symmetries of the space [1], [11]–[14]. The theory of invariant observer design is based on the estimation error being invariant under the action of a matrix Lie group, leading to constant linearizations, linear observability analysis, and convergence property for the deterministic group-affine systems [7], [15], [16]; hence, we adopt this framework here.

One challenge for robot state estimation is the slip incurred by uneven, deformable, or low friction terrains. Once a slip happens, it violates the fixed contact point assumption, thus resulting in drifts. Another interesting aspect of detecting slip is stability control. If one could detect slip as accurately, the controller can then use this information to maintain robot stability [17], [18].

In this work, we develop a novel slip estimator using a Right Invariant Extended Kalman Filter (RI-EKF). The proposed model estimates the body slip velocity in the world frame by treating it as a bias in the velocity measurements.

Toyota Research Institute provided funds to support this work. Funding for M. Ghaffari was in part provided by NSF Award No. 2118818.

X. Yu, S. Teng, T. Chakhachiro, W. Tong, T. Li, T.Y. Lin and M. Ghaffari are with the University of Michigan, Ann Arbor, MI 48109, USA. {xihangyu, sanglit, teochiro, wenzhet}@umich.edu, {tingjunl, tzuyuan, maanigj}@umich.edu

S. Koehler, M. Ahumada, and J. Walls are with Woven Planet. {sarah.koehler, manuel.ahumada}@woven-planet.global, jeff.walls@woven-planet.global



Fig. 1: Experimental wheeled robot platform Husky. The world frame  $W$  is a fixed frame. We define the body frame  $B$  as  $x$  pointing forward,  $y$  point to the left of the vehicle, and  $z$  derived from the right hand rule. We obtain angular velocity measurements  $\omega_l$  and  $\omega_r$  from the wheel encoders. Using an inertial measurement unit and wheel encoders measurements, the proposed method estimates the body velocity, slip velocity, robot orientation and position, visualized as  $v$ ,  $u$ ,  $R$ , and  $p$ , respectively.

Given the encoder-inertial data on wheeled platforms, the slip velocity can be estimated in a fully proprioceptive manner. In particular, this work has the following contributions.

- 1) A real-time RI-EKF state and slip estimator for wheeled mobile robots using only onboard encoder-inertial measurements.
- 2) A slip event observer as a binary classifier using Chi-square statistical test.
- 3) Experimental results using a Husky robot on multiple terrains to verify the mathematical derivations and validate the effectiveness of the proposed state estimator.
- 4) Open source software is available for download at [https://github.com/UMich-CURLY/slip\\_detection\\_DOB](https://github.com/UMich-CURLY/slip_detection_DOB)

## II. RELATED WORK

Direct measurements, e.g., using biomimetic tactile sensors [19], [20], can provide slip detection; however, specialized hardware is required, and such sensors can be too fragile for mobile robots. Therefore, algorithmic methods based on limited sensing data are attractive solutions for slip detection.

### A. Model-based methods

The work of [21] designs a slip controller on a six-wheel mobile robot to perform obstacle climbing maneuvers. Slip is detected by comparing the wheel velocity from the forward kinematics with the body velocity estimated by the visual-inertial system. A slip event is classified as true if the normalized difference is larger than a fixed threshold. The work of [22] fuses multiple models for wheel slip prediction

in a nonlinear observer. For instantaneous slip detection, this work requires the visual measurement or the wheel motor current. Then a more complicated slip detection model is incorporated to predict the slip events. These methods rely on accurate body velocity estimation from a camera or privileged information of the friction profile, whereas the proposed work here is fully proprioceptive.

Other than fusing kinematics or visual data, more work used the dynamics model of the vehicles for state estimation. [23] fuses the simplified vehicle dynamics, kinematics models and tire models to estimate the *slip angle*, i.e. the angle between the vehicle heading direction and actual velocity. The slip angle is crucial for friction coefficient and slip estimation. The work of [24] uses the full dynamics of the vehicle and tire models to estimate the longitudinal and lateral speed of the vehicles using a nonlinear observer. Based on [24], the work of [25] applied a update law to the friction parameters so the nonlinear observer could adapt to varying friction condition. However, the work in [23]–[25] rely on vehicle dynamics model, assumes known terrain inclinations or certain friction parameters. In our methods, we only assume the kinematics model and do not have any assumption on the terrain inclination or friction.

### B. Learning-based methods

The work of [26] uses the Support Vector Machine (SVM) for slip detection. An in-wheeled sensor is used to measure the normal force and contact angle. The work of [27], [28] explored various learning algorithms to estimate slip for wheeled robots—these methods model the slip estimation task as a classification problem. The main drawback of the supervised learning-based method is that ground truth is hard to obtain. In [26], the ground truth is hand labeled, which is laborious and prone to error. Although [27] does not rely on hand labeling data, the experiment is conducted in a laboratory environment using a single wheel. The ground truth is obtained by measuring the wheel’s angular velocity and the carriage pulley’s angular velocity. The work of [28] uses other sensors such as GPS for ground truthing, which suffers from outages (i.e., indoors or shaded areas). The work of [29] models slip detection as an unsupervised learning problem. However, the slip detection is modeled as classification, leading to inaccessible slip velocities.

The reinforcement learning-based system identification has also drawn attention recently. [30] trained a network in the simulator to estimate the unknown parameters of mechanical models for control. The Rapid Motor Adaptation [31], [32] has been applied to legged robot control by encoding the environmental factors to latent spaces. The environment factor encoder enables online system identification for varying environments. However, the learned high dimensional latent space lacks interpretability. In this work, we develop a low dimensional slip model that can be estimated recursively without the need for offline training.

### C. Filtering-based methods

The contact-aided InEKF [7] fuses the foot contact state, forward kinematics and Inertial Measurement Unit (IMU) measurements, assuming the contact point being fixed in the world frame. For legged robot state estimation on slippery terrain, [33] applied the UKF to fuse the end-effector velocity and a Chi-square detection to discard unreliable measurements when the foot is not static. The discarding method enables more robust performance, but also reduces the number of measurements. The work of [34] fuses visual-based velocity measurement with leg kinematics and inertial measurements on slippery terrain. The incorporation of visual information can compensate for the unreliable measurements from leg kinematics. The above methods either assume static contact point or treat slip events as outliers.

The Disturbance Observer (DOB) estimates the disturbance by explicitly representing it as a new state variable [35], [36]. The DOB does not assume accurate dynamics of the disturbances but uses simple dynamics with higher generalizability. In this work, we model the slip velocity as an exponentially decaying variable, i.e., an autoregressive process, which is simple yet can capture the core dynamics of slippage. Compared to previous works, we address the problem of slip velocity estimation using a lightweight DOB that is fully proprioceptive.

## III. MATHEMATICAL PRELIMINARY AND NOTATION

We assume a matrix Lie group denoted  $\mathcal{G}$  and its associated Lie Algebra denoted  $\mathfrak{g}$ . Let  $(\cdot)^\wedge : \mathbb{R}^{\dim \mathfrak{g}} \rightarrow \mathfrak{g}$  be the linear map that takes elements of the tangent space of  $\mathcal{G}$  at the identity to the corresponding matrix representation so that  $\exp : \mathbb{R}^{\dim \mathfrak{g}} \rightarrow \mathcal{G}$ , is computed by  $\exp(\xi) = \exp_m(\xi^\wedge)$ , where  $\exp_m(\cdot)$  is the usual exponential of  $n \times n$  matrices. A process dynamics evolving on the Lie group with state at time  $t$ ,  $X_t \in \mathcal{G}$ , is denoted by  $\frac{d}{dt}X_t = f_{u_t}(X_t)$ , and  $\hat{X}_t$  is used to denote an estimate of the state.

**Definition 1** (Right-Invariant Error). *The right-invariant error between two trajectories  $X_t$  and  $\hat{X}_t$  is:*

$$\eta_t^r = \hat{X}_t X_t^{-1} = (\hat{X}_t L)(X_t L)^{-1}, \quad (1)$$

where  $L$  is an arbitrary element of the group.

The following two theorems are the fundamental results for deriving an InEKF.

**Theorem 1** (Autonomous Error Dynamics [15]). *A system is group affine if the dynamics,  $f_{u_t}(\cdot)$ , satisfies:*

$$f_{u_t}(X_1 X_2) = f_{u_t}(X_1) X_2 + X_1 f_{u_t}(X_2) - X_1 f_{u_t}(I_d) X_2, \quad (2)$$

for all  $t > 0$  and  $X_1, X_2 \in \mathcal{G}$ . Furthermore, if this condition is satisfied, the right-invariant error dynamics are trajectory independent and satisfy:

$$\frac{d}{dt} \eta_t^r = g_{u_t}(\eta_t^r) \quad \text{where} \quad g_{u_t}(\eta^r) = f_{u_t}(\eta^r) - \eta^r f_{u_t}(I_d).$$

The group identity element is denoted  $I_d \in \mathcal{G}$ ; we use  $I$  for a  $3 \times 3$  identity matrix, and  $I_n$  for the  $n \times n$  case.

Define  $A_t$  to be a  $\dim_{\mathfrak{g}} \times \dim_{\mathfrak{g}}$  matrix satisfying  $g_{u_t}(\exp(\xi)) := (A_t \xi)^\wedge + \mathcal{O}(\|\xi\|^2)$ . For all  $t \geq 0$ , let  $\xi_t$  be the solution of the linear differential equation

$$\frac{d}{dt} \xi_t = A_t \xi_t. \quad (3)$$

**Theorem 2** (Log-Linear Property of the Error [15]). *Consider the right-invariant error,  $\eta_t$ , between two trajectories (possibly far apart). For arbitrary initial error  $\xi_0 \in \mathbb{R}^{\dim_{\mathfrak{g}}}$ , if  $\eta_0 = \exp(\xi_0)$ , then for all  $t \geq 0$ ,  $\eta_t = \exp(\xi_t)$ ; that is, the nonlinear estimation error  $\eta_t$  can be exactly recovered from the time-varying linear differential equation (3).*

We work with a right-invariant observation model that leads to the autonomous linearized observation model and innovation [15].

$$Y_t = X_t^{-1} b + n_t \quad (\text{Right-Invariant Observation}), \quad (4)$$

where  $b$  is a constant vector and  $n_t$  is a vector of Gaussian noise. Finally, for any  $X \in \mathcal{G}$  the adjoint map,  $\text{Ad}_X : \mathfrak{g} \rightarrow \mathfrak{g}$ , is a linear map defined as  $(\text{Ad}_X \xi)^\wedge = X \xi^\wedge X^{-1}$ . The similarity transformation via the adjoint allows change of frame on the Lie group manifold.

#### IV. SYSTEM MODELS

In this section, we introduce the kinematics model of the differential wheeled robot and derive the dynamics of wheel slip velocity. For a quantity  $\zeta$ , we use  $\tilde{\zeta}$  to denote its measurement and  $\hat{\zeta}$  to indicate its estimation.

##### A. IMU model

The state of the IMU can be represent by its orientation  $R \in \text{SO}(3)$ , velocity  $v \in \mathbb{R}^3$ , and position  $p \in \mathbb{R}^3$  in the world frame [7]. The IMU measures the acceleration  $a \in \mathbb{R}^3$  and angular velocity  $\omega \in \mathbb{R}^3$  in the IMU frame. Consider the white Gaussian noise in the gyroscope  $w_\omega \sim \mathcal{N}(0_3, \Sigma^\omega)$  and accelerometer  $w_a \sim \mathcal{N}(0_3, \Sigma^a)$ , the IMU measurements can be represented by  $\tilde{\omega} = \omega + w_\omega$ ,  $\tilde{a} = a + w_a$ . Given the IMU measurements, its unbiased dynamics can be represent as

$$\dot{R} = R(\tilde{\omega} - w_\omega)^\wedge, \quad \dot{v} = R(\tilde{a} - w_a) + g, \quad \dot{p} = v, \quad (5)$$

where  $g$  is the gravity vector. For bias augmentation and discretization of the system, we follow the same approach as that of [7].

##### B. Differential wheel robot model

The angular velocities of left and right wheel around their axes, i.e.,  $\omega_l, \omega_r \in \mathbb{R}$ , can be measured by the encoders. Let  $q \in \mathbb{R}$  be the known wheel radius. Assuming zero velocity at the contact points, the forward velocities of the wheel radius centers are  $\tilde{v}_{xl} = \omega_l q$  and  $\tilde{v}_{xr} = \omega_r q$ .

Due to the nonholonomic constraints of the wheels, we assume that the robot has zero lateral and vertical velocity. This pseudo-measurement model has been used previously in [37], [38]. For differential wheel robot, there is one additional constraint in forward velocity that the forward velocity is the average of velocities for left and right wheel radius centers.

Combining all measurements, we form the observation model without slip estimation as

$$y_{ENC} := \text{vec} \left( \frac{1}{2} (\tilde{v}_{xl} + \tilde{v}_{xr}), 0, 0 \right) = R^\top v. \quad (6)$$

##### C. Wheel slip model

The differential wheel kinematics in IV-B assumes the non-slip condition, which may not be valid when slip happens. Inspired by the DOB, we explicitly model the slip velocity as a new state variable. Let  $u \in \mathbb{R}^3$  be the slip velocity (disturbance) in world frame. We append  $u$  to (6) and we have the new observation model:

$$y_{ENC} = R^\top v + R^\top u + w_y, \quad (7)$$

where  $w_y \sim \mathcal{N}(0_3, W_y)$  is a lumped zero-mean white Gaussian noise term that takes into account the uncertainty in kinematics model, slip events, and encoders.

The philosophy of DOB is that we can use a simple model to represent the dynamics of disturbance. One widely adopted method is to model the disturbance as a constant. However, this model does not match the reality as the slip event dissipates energy. Instead, we use an autoregressive process to model it. Thus, the dynamics of slip compensation in the world frame is modeled as follows.

$$\dot{u} = -\alpha u + R w_u, \quad w_u \sim \mathcal{N}(0_3, \Sigma^u), \quad (8)$$

where  $\alpha > 0$  indicates the decaying rate of the slip velocity. Here we consider  $w_u$  as a lumped noise term that represent the uncertainty of the slip model and other random effect.

**Remark 1.** *Suppose the robot is slipping on icy ground. After gaining an initial momentum and without any external forces other than friction, the robot will slip forward with a decreasing velocity in the world frame and eventually stop. This observation inspires the above autoregressive process.*

#### V. THE INVARIANT EXTENDED KALMAN FILTERING

##### A. State representation on Lie group

Define the state matrix on the Lie group  $\text{SE}_3(3)$  as:

$$X = \begin{bmatrix} R & v & p & u \\ 0_{3,3} & I & & \end{bmatrix} \in \text{SE}_3(3). \quad (9)$$

The Lie Algebra  $\mathfrak{se}_3(3)$  of above Lie group  $\text{SE}_3(3)$ , is a 12-dimensional vector space. The continuous-time noisy process dynamics,  $\frac{d}{dt} X =: f_{u_t}(X) - X w_t^\wedge$  is given by

$$\frac{d}{dt} X = \begin{bmatrix} R \tilde{\omega}^\wedge & R \tilde{a} + g & v & -\alpha u \\ 0_{3,3} & 0_{3,1} & 0_{3,1} & 0_{3,1} \end{bmatrix} - X w_t^\wedge. \quad (10)$$

##### B. InEKF Propagation Step

The system dynamics satisfy the group affine property, according to Theorems 1 and 2; thus, the dynamics of the state estimation error is autonomous and the linearized system is independent of the system states.

Define  $w_t := \text{vec}(w_\omega, w_a, 0_{3 \times 1}, w_u)$  and the linearized state estimation error  $\xi := \text{vec}(\xi_R, \xi_v, \xi_p, \xi_u) \in \mathbb{R}^{12}$ .

Then we have the linear error dynamic system  $\frac{d}{dt}\xi_t = A\xi_t + \text{Ad}_{\hat{X}_t} w_t$ , where

$$A = \begin{bmatrix} 0_3 & 0_3 & 0_3 & 0_3 \\ g^\wedge & 0_3 & 0_3 & 0_3 \\ 0_3 & I_3 & 0_3 & 0_3 \\ 0_3 & 0_3 & 0_3 & -\alpha I_3 \end{bmatrix}, \quad (11)$$

and  $\text{Ad}_{\hat{X}_t}$  is the group adjoint map [7]. The covariance of the augmented right invariant error dynamics is computed by solving the Riccati equation  $\frac{d}{dt}P_t = A_t P_t + P_t A_t^\top + \hat{Q}_t$ , where  $\hat{Q}_t = \text{Ad}_{\hat{X}_t} \text{Cov}(w_t) \text{Ad}_{\hat{X}_t}^\top$ .

### C. Right-Invariant Correction Step

We can re-write (7) as a right-invariant observation model,  $y = \hat{X}^{-1}b + n$ , where  $y := \text{vec}(\frac{1}{2}(\tilde{v}_l + \tilde{v}_r), -1, 0, -1)$ ,  $b := \text{vec}(0_{1 \times 3}, -1, 0, -1)$ , and  $n := \text{vec}(w_y, 0, 0, 0)$ . Then we compute the right-invariant measurement Jacobian,  $H$ , using  $H\xi^r = -(\xi^r)^\wedge b$  as  $H = [0_3, I, 0_3, I]$ .

Following RI-EKF methodology [7], [15], we can compute the innovation covariance  $S = HPH^\top + W_y$  and the filter gain  $K = PH^\top S^{-1}$ . Let  $\Pi := [I, 0_3]$  be a column selection matrix. We then compute an updated state and covariance, using  $\hat{X}^+ = \exp(K\Pi(\hat{X}y - b))\hat{X}$  and  $P^+ = (I_{12} - KH)P$ , respectively.

### D. Observability Analysis

Because the error dynamics are log-linear (c.f., Theorem 2), we can determine the unobservable states of the filter without nonlinear observability analysis [39]. Noting that the linear error dynamics matrix in our case is time-invariant and nilpotent (with a degree of three), the discrete-time state transition matrix,  $\Phi = \exp_m(A\Delta t)$ , is

$$\Phi = \begin{bmatrix} I & 0 & 0 & 0 \\ (g)^\times \Delta t & I & 0 & 0 \\ \frac{1}{2}(g)^\times \Delta t^2 & I\Delta t & I & 0 \\ 0 & 0 & 0 & \exp(-\alpha I\Delta t) \end{bmatrix}.$$

It follows that the discrete-time observability matrix is

$$\mathcal{O} = \begin{bmatrix} H \\ H\Phi \\ H\Phi^2 \\ \vdots \end{bmatrix} = \begin{bmatrix} 0 & I & 0 & I \\ (g)^\times \Delta t & I & 0 & \exp(-\alpha I\Delta t) \\ 2(g)^\times \Delta t & I & 0 & \exp(-\alpha I\Delta t)^2 \\ \vdots & \vdots & \vdots & \vdots \end{bmatrix}.$$

The second last column (i.e., one matrix column) of the observability matrix are zeros, indicating the absolute position of the robot, which is unobservable. Because the gravity vector only has a  $z$  component, a rotation about the gravity vector (yaw) is also unobservable. Moreover, we note that slip disturbances are fully observable except for  $\alpha = 0$ .

### E. Chi-square hypothesis testing for slip detection

To classify slip events, we use the Chi-Square hypothesis testing. Note that we have modeled the dynamics of slip velocity  $u$  as an autoregressive process in (8). Therefore,  $u$  is exponentially stable, and its covariance has a bounded steady state value for a bounded noise input. From the property of exponential stability, the mean value of  $u$  converges to a

TABLE I: Noise Parameters and initial Covariances. All values show the standard deviations, and covariances are spherical.

Measurement Type	Noise std. dev.	State Variable	Initial Covariance
Gyroscope	0.1 rad/s	Robot Orientation	0.03 rad
Accelerometer	0.1 m/s <sup>2</sup>	Robot Velocity	0.01 m/s
Gyroscope Bias	0.001 rad/s	Robot Position	0.01 m
Accelerometer Bias	0.001 m/s <sup>2</sup>	Robot Slip Velocity	0.01 m/s
Wheel Encoder Vel	0.1 m/s	Gyroscope Bias	0.0001 rad/s
Disturbance Process	5 m/s	Accelerometer Bias	0.0025 m/s <sup>2</sup>

steady state  $\mathbb{E}[u] =: \bar{u} = 0$  and the covariance converges to a steady state value  $\text{Cov}(\bar{u}) =: \Sigma_{\bar{u}}$ . The steady state covariance of  $u$  is unknown and does not necessarily equal the time-varying covariance estimated by the filter. As such, we test if  $u$  matches an empirical steady-state distribution  $\mathcal{N}(0, \Sigma_{\bar{u}})$  using a Chi-square test, where we manually tune  $\Sigma_{\bar{u}}$  in this work to be a constant covariance matrix. We compute the Chi-square statistics with  $n = 3$  degrees of freedom as:

$$r := (u - \bar{u})^\top \Sigma_{\bar{u}}^{-1} (u - \bar{u}) = u^\top \Sigma_{\bar{u}}^{-1} u \sim \chi_{n=3}^2. \quad (12)$$

If  $r$  is larger than a threshold given a confidence level, we consider the robot state as slipping; otherwise, non-slipping. In the experiment in Sec. VI, we set the steady state covariance as  $\Sigma_{\bar{u}} = 0.001 \cdot I$ . A threshold value of 4.642 is used for a probability value 0.80 and 3 degrees of freedom from the Chi-square distribution table. If the observed value is larger than this threshold, we consider it an outlier, and a slip event occurs.

## VI. EXPERIMENTAL RESULTS

We conduct two experiments to validate the proposed methods on a Husky robot as shown in Fig. 1. In the first experiment, the robot moves over a highly slippery soap area back and forth. In the second experiment, the robot climbs onto a sandy hill twice. With these two test sequences, we focus on evaluating the performance of the proposed method on velocity and orientation estimation, as well as slip detection. For the tracking results of the InEKF on the Husky platform see [40].

As we test our method in the outdoor area without a motion capture system, we use a state-of-the-art visual SLAM system, ORB-SLAM3 [41], to serve as a proxy for the ground truth velocity. The images used in ORB-SLAM3 are streamed from a ZED camera mounted on top of the robot. The camera is used for ground truth generation only. The proposed method is fully proprioceptive with the IMU measurements arriving at 200 Hz, and the encoder data at 13.5 Hz. In addition to the proposed method, we run the InEKF without the DOB as a baseline algorithm. The measurement noise statistics and initial covariance estimates are provided in Table I. We fixed hyperparameters in all experiments (including both baseline and proposed filters) for better comparison.

### A. DOB as State Estimator

We use the observation model described in (7) to correct the predicted states. However, instead of setting a constant measurement covariance,  $W_y$ , we make  $W_y$  adaptive based

TABLE II: RMSE comparison between the baseline (InEKF) and the proposed filter (InEKF w/ DOB) in the experiment of Sec. VI-A. We compute the RMSE error during 44 sec–57 sec with respect to each rotation (in rad) and velocity (in m/sec) axis.

State	yaw	pitch	roll	$v_x$	$v_y$	$v_z$
InEKF	0.098	0.018	0.027	0.155	<b>0.052</b>	0.039
InEKF w/ DOB	0.098	<b>0.008</b>	<b>0.015</b>	<b>0.100</b>	0.055	<b>0.036</b>



Fig. 2: The Husky robot is navigating on a highly slippery soap-covered tape ground (black areas).

on the estimated slip velocity, i.e.,

$$W_y = W_0 \exp(\|u\|). \quad (13)$$

Here,  $W_0$  is the initial covariance that corresponds to the covariance when no slip is present. When the robot is suffering from severe slip, the measurement covariance increases exponentially with respect to the estimated slip velocity.

In the first experiment, Husky moves on a soapy surface back and forth, as demonstrated in Fig. 2. Fig. 3 plots the estimated orientation and velocity in this sequence. We focus on the period from 44 sec to 57 sec, in which the robot moves through the slippery area.<sup>1</sup> For attitude estimation, yaw angle is unobservable as pointed out in observability analysis.

Root Mean Square Error (RMSE) comparison between the baseline and the proposed filter is presented in Table II. The proposed algorithm performs better than the baseline pitch and roll estimation, which are essential for vehicle stability, especially in off-road scenarios. The disturbance observer provides accurate attitude estimation in the slippery area. For body velocity estimation, the proposed algorithm outperforms the baseline algorithm in the  $x$ -axis (dominant dimension of the signal here), and there is a slight improvement in the  $z$  direction. However, in the  $y$ -axis, estimated velocity from the original InEKF [40] performs slightly better. We conjecture this is due to inappropriate covariance adaptation by (13).

### B. DOB as Slip Event Observer

Disturbance observer also serves as a slip-aware filter. We use a Chi-square hypothesis test to classify slip states as binary events. We manually label ground truth data. When the robot turns around or moves through the soap area, we consider it a slip event, while on normal ground, we consider it non-slip. We show the result of the Chi-square test in the

<sup>1</sup>The rosbag of this dataset can be found on our GitHub page.

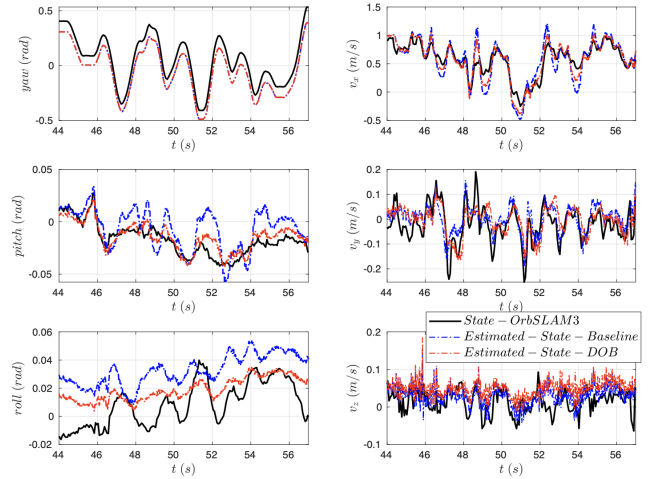


Fig. 3: Yaw, pitch and roll angles of the main body are depicted in the left three figures. Body Velocities are depicted in the right three figures. Black lines: ground truth from ORB-SLAM3 system. Blue dashed: plain InEKF without DOB. Red dashed: InEKF with DOB. Note that the ORB-SLAM3 algorithm only provides the pose estimation. The velocity is the result of differentiating the estimated pose.

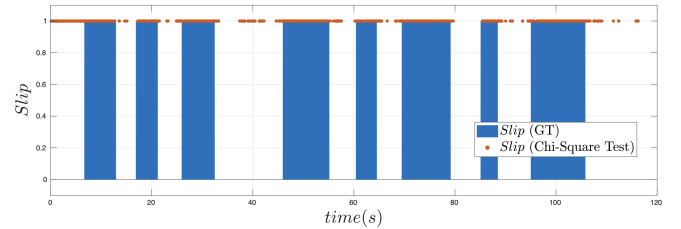


Fig. 4: Slip state estimation from sequence over slippery soap terrain. We use 1 for slipping and 0 for non-slipping. Red dots: Detected slip event during which robot is slipping. Blue bars: Ground truth during which robot is slipping.

120-second sequence in row 1 of Fig. 4, we set  $\chi^2$  confidence level at 80% and the corresponding threshold as 4.642.

We achieve about 77.32% accuracy (Fig. 2) as shown in Table III. Furthermore, there is 20.33% False Positive Rate (FPR), i.e, detected slip but in reality not a slip event, and 25.60% False Negative Rate (FNR), i.e., slip events that are not detected.

### C. Experiment on Highly Deformable Terrain

The second experiment is conducted outdoors on a deformable terrain. As illustrated in Fig. 5, the Husky was driven twice straight up to a hill covered with sand. Fig. 6 shows this estimated velocity and disturbance of this sequence. Compared to the baseline method, the proposed algorithm provides more accurate velocity estimations when Husky is experiencing severe slipping (seconds 8-12 and seconds 18-22). The quantitative results of this sequence are shown in Table IV. The proposed filter outperforms standard InEKF in all three velocity directions while keeping similar results in orientation. Slip velocity estimation is shown in the right three subplots in Fig. 6. The two peaks in the  $x$  and  $z$  directions represent severe slipping when the robot is on the slope of the hill. We observe that the peaks of the  $z$ -axis appear at second 8 and second 18 because at those moments robot is at the highest slope on the hill. Peaks of the  $x$ -axis appear later at second 11 and second 21 when



Fig. 5: A sequence of snapshots illustrating the substantial slip that is occurring during the experiment. If looking at the contact points of the right rear wheel with ground, one can observe that sands are rolling behind when the wheel is rotating.

TABLE III: The average performance of the proposed filter (InEKF w/ DOB) in slip estimation.

Experiment	FPR	FNR	Accuracy
Artificial slippery terrain	20.33%	25.60%	77.32%
Deformable sand terrain	59.14%	7.78%	65.76%

TABLE IV: RMSE comparison between the baseline (InEKF) and the proposed filter (InEKF w/ DOB) in the experiment of Sec. VI-C.

State	yaw	pitch	roll	$v_x$	$v_y$	$v_z$
InEKF	0.046	<b>0.056</b>	0.035	0.305	0.092	0.140
InEKF w/ DOB	0.046	0.057	0.035	<b>0.277</b>	<b>0.087</b>	<b>0.077</b>

the robot returns to the low-slope valley. To validate the proposed method as slip detector, we run the Chi-square test in Sec. VI-B. Quantitative results are shown in Table III. Slip ground truth is labeled manually using the tire tracks.

## VII. DISCUSSION AND LIMITATIONS

In this work, we model the slip velocity of the whole body frame within a RI-EKF framework. A more precise model is to estimate the slip velocity of left and right wheels separately. However, these states are not observable using only encoders and IMU data. Currently, the decaying rate  $\alpha$  should be tuned by hand. However, the value of hyperparameter should reflect the ground-tire friction coefficient (i.e., for more slippery terrain, the alpha should be smaller). It is known that the knowledge of the friction dynamics can improve the vehicle's model fidelity [42]. Our proposed filter might be used in friction coefficient identification. The covariance matrix of encoder measurements is set heuristically in the InEKF and updated adaptively by a manually designed function. This can cause inaccuracy sometimes as in the  $v_y$  estimation in Fig. 3. In the future, we wish to use learning to estimate the covariance of the current measurements [38]. This approach will allow the state estimator to fully exploit the information in disturbance estimation. Moreover, the steady state distribution for the disturbance is also set heuristically in the Chi-Square test. This value could potentially also be learned by a neural network. Finally, the developed slip disturbance observer

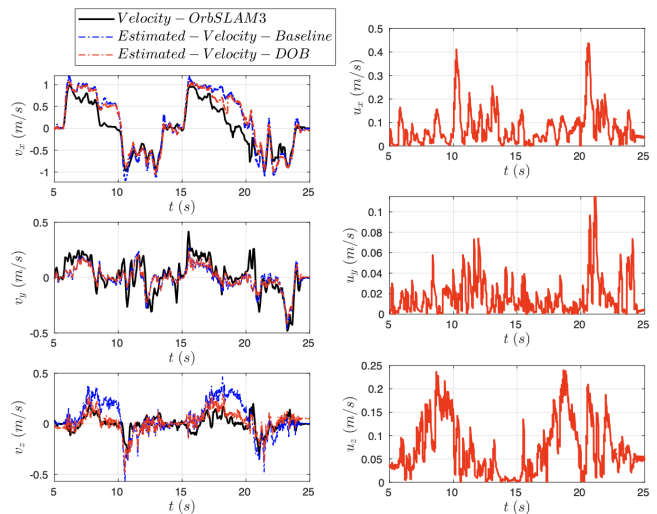


Fig. 6: Estimated velocity and disturbance for the hill sequence. Note that the estimated velocity and disturbance are represented in the world frame. Left 3 figures plot the estimated velocities from the proposed method (Red), the baseline (Blue), and the ground truth velocity from ORB-SLAM3 (Black). Right 3 figures present the estimated slip velocities from the proposed method. The two peaks in  $x$  and  $z$  directions represent severe slipping when robot is on the slope of the hill.

could be integrated into other platforms, such as legged robots, where the body velocity measurements are used [43].

## VIII. CONCLUSION

We developed a lightweight filtering-based slip velocity estimation method that only uses encoder and IMU data and works in real time on distinct terrains. In addition, a Chi-Square hypothesis testing approach is proposed for detecting slip events. We tested the proposed algorithm on a Husky wheeled robot and demonstrate better performance than a standard InEKF. The discussed limitations motivate future study in this area of robot state estimation. The proposed slip velocity estimator is a low-cost addition to the existing invariant EKF and has the potential to be widely adopted on various robotic platforms.

## REFERENCES

- [1] T. D. Barfoot, *State estimation for robotics*. Cambridge University Press, 2017.
- [2] Y. Gong and J. Grizzle, “One-step ahead prediction of angular momentum about the contact point for control of bipedal locomotion: Validation in a LIP-inspired controller,” in *Proceedings of the IEEE International Conference on Robotics and Automation*. IEEE, 2021, pp. 2832–2838.
- [3] A. Agrawal, S. Chen, A. Rai, and K. Sreenath, “Vision-aided dynamic quadrupedal locomotion on discrete terrain using motion libraries,” in *Proceedings of the IEEE International Conference on Robotics and Automation*. IEEE, 2022, pp. 4708–4714.
- [4] S. Teng, D. Chen, W. Clark, and M. Ghaffari, “An error-state model predictive control on connected matrix Lie groups for legged robot control,” in *Proceedings of the IEEE/RSJ International Conference on Intelligent Robots and Systems*. IEEE, 2022, pp. 1–8.
- [5] L. Gan, J. W. Grizzle, R. M. Eustice, and M. Ghaffari, “Energy-based legged robots terrain traversability modeling via deep inverse reinforcement learning,” *IEEE Robotics and Automation Letters*, vol. 7, no. 4, pp. 8807–8814, 2022.
- [6] S. Teng, W. Clark, A. Bloch, R. Vasudevan, and M. Ghaffari, “Lie algebraic cost function design for control on Lie groups,” *arXiv preprint arXiv:2204.09177*, 2022.
- [7] R. Hartley, M. Ghaffari, R. M. Eustice, and J. W. Grizzle, “Contact-aided invariant extended Kalman filtering for robot state estimation,” *International Journal of Robotics Research*, vol. 39, no. 4, pp. 402–430, 2020.
- [8] T.-Y. Lin, R. Zhang, J. Yu, and M. Ghaffari, “Legged robot state estimation using invariant Kalman filtering and learned contact events,” in *5th Annual Conference on Robot Learning*, 2021.
- [9] Y. Gao, C. Yuan, and Y. Gu, “Invariant filtering for legged humanoid locomotion on dynamic rigid surfaces,” *arXiv preprint arXiv:2201.10636*, 2022.
- [10] P. van Goor and R. Mahony, “EqVIO: An equivariant filter for visual inertial odometry,” *arXiv preprint arXiv:2205.01980*, 2022.
- [11] G. S. Chirikjian, *Stochastic Models, Information Theory, and Lie Groups, Volume 2: Analytic Methods and Modern Applications*. Springer Science & Business Media, 2011.
- [12] A. W. Long, K. C. Wolfe, M. J. Mashner, and G. S. Chirikjian, “The banana distribution is Gaussian: A localization study with exponential coordinates,” *Proceedings of the Robotics: Science and Systems Conference*, vol. 265, 2013.
- [13] T. D. Barfoot and P. T. Furgale, “Associating uncertainty with three-dimensional poses for use in estimation problems,” *IEEE Transactions on Robotics*, vol. 30, no. 3, pp. 679–693, 2014.
- [14] B. Hall, *Lie groups, Lie algebras, and representations: an elementary introduction*. Springer, 2015, vol. 222.
- [15] A. Barrau and S. Bonnabel, “The invariant extended Kalman filter as a stable observer,” *IEEE Transactions on Automatic Control*, vol. 62, no. 4, pp. 1797–1812, 2017.
- [16] —, “Invariant Kalman filtering,” *Annual Review of Control, Robotics, and Autonomous Systems*, 2018.
- [17] N. D. Wallace, H. Kong, A. J. Hill, and S. Sukkarieh, “Receding horizon estimation and control with structured noise blocking for mobile robot slip compensation,” in *Proceedings of the IEEE International Conference on Robotics and Automation*. IEEE, 2019, pp. 1169–1175.
- [18] G. Bledt, P. M. Wensing, S. Ingersoll, and S. Kim, “Contact model fusion for event-based locomotion in unstructured terrains,” in *Proceedings of the IEEE International Conference on Robotics and Automation*. IEEE, 2018, pp. 4399–4406.
- [19] J. W. James, N. Pestell, and N. F. Lepora, “Slip detection with a biomimetic tactile sensor,” *IEEE Robotics and Automation Letters*, vol. 3, no. 4, pp. 3340–3346, 2018.
- [20] J. Li, S. Dong, and E. Adelson, “Slip detection with combined tactile and visual information,” in *Proceedings of the IEEE International Conference on Robotics and Automation*. IEEE, 2018, pp. 7772–7777.
- [21] N. Pico, H.-R. Jung, J. Medrano, M. Abayebas, D. Y. Kim, J.-H. Hwang, and H. Moon, “Climbing control of autonomous mobile robot with estimation of wheel slip and wheel-ground contact angle,” *J. Mech. Sci. Technol.*, vol. 36, no. 2, pp. 959–968, Feb. 2022.
- [22] M. T. Malinowski, A. Richards, and M. Woods, “Wheel slip prediction for improved rover localization,” in *AIAA SCITECH 2022 Forum*. Reston, Virginia: American Institute of Aeronautics and Astronautics, Jan. 2022.
- [23] D. Piyabongkarn, R. Rajamani, J. A. Grogg, and J. Y. Lew, “Development and experimental evaluation of a slip angle estimator for vehicle stability control,” *IEEE Transactions on control systems technology*, vol. 17, no. 1, pp. 78–88, 2008.
- [24] L. Imsland, T. A. Johansen, T. I. Fossen, H. F. Grip, J. C. Kalkkuhl, and A. Suissa, “Vehicle velocity estimation using nonlinear observers,” *Automatica*, vol. 42, no. 12, pp. 2091–2103, 2006.
- [25] H. F. Grip, L. Imsland, T. A. Johansen, T. I. Fossen, J. C. Kalkkuhl, and A. Suissa, “Nonlinear vehicle side-slip estimation with friction adaptation,” *Automatica*, vol. 44, no. 3, pp. 611–622, 2008.
- [26] T. Omura and G. Ishigami, “Wheel slip classification method for mobile robot in sandy terrain using in-wheel sensor,” *Journal of Robotics and Mechatronics*, vol. 29, no. 5, pp. 902–910, 2017.
- [27] R. Gonzalez and K. Iagnemma, “Deepterramechanics: Terrain classification and slip estimation for ground robots via deep learning,” *arXiv preprint arXiv:1806.07379*, 2018.
- [28] R. Gonzalez, D. Apostolopoulos, and K. Iagnemma, “Slippage and immobilization detection for planetary exploration rovers via machine learning and proprioceptive sensing,” *Journal of Field Robotics*, vol. 35, no. 2, pp. 231–247, 2018.
- [29] M.-R. Bouguelia, R. Gonzalez, K. Iagnemma, and S. Byttner, “Unsupervised classification of slip events for planetary exploration rovers,” *Journal of Terramechanics*, vol. 73, pp. 95–106, 2017.
- [30] W. Yu, J. Tan, C. K. Liu, and G. Turk, “Preparing for the unknown: Learning a universal policy with online system identification,” *arXiv preprint arXiv:1702.02453*, 2017.
- [31] A. Kumar, Z. Fu, D. Pathak, and J. Malik, “RMA: Rapid motor adaptation for legged robots,” *arXiv preprint arXiv:2107.04034*, 2021.
- [32] A. Kumar, Z. Li, J. Zeng, D. Pathak, K. Sreenath, and J. Malik, “Adapting rapid motor adaptation for bipedal robots,” *arXiv preprint arXiv:2205.15299*, 2022.
- [33] M. Bloesch, C. Gehring, P. Fankhauser, M. Hutter, M. A. Hoepfner, and R. Siegwart, “State estimation for legged robots on unstable and slippery terrain,” in *Proceedings of the IEEE/RSJ International Conference on Intelligent Robots and Systems*. IEEE, 2013, pp. 6058–6064.
- [34] S. Teng, M. W. Mueller, and K. Sreenath, “Legged robot state estimation in slippery environments using invariant extended Kalman filter with velocity update,” in *Proceedings of the IEEE International Conference on Robotics and Automation*. IEEE, 2021, pp. 3104–3110.
- [35] W.-H. Chen, J. Yang, L. Guo, and S. Li, “Disturbance-observer-based control and related methods - an overview,” *IEEE Transactions on industrial electronics*, vol. 63, no. 2, pp. 1083–1095, 2015.
- [36] J. Han, “From PID to active disturbance rejection control,” *IEEE transactions on Industrial Electronics*, vol. 56, no. 3, pp. 900–906, 2009.
- [37] G. Dissanayake, S. Sukkarieh, E. Nebot, and H. Durrant-Whyte, “The aiding of a low-cost strapdown inertial measurement unit using vehicle model constraints for land vehicle applications,” *IEEE Transactions on Robotics and Automation*, vol. 17, no. 5, pp. 731–747, 2001.
- [38] M. Brossard, A. Barrau, and S. Bonnabel, “AI-IMU dead-reckoning,” *IEEE Transactions on Intelligent Vehicles*, vol. 5, no. 4, pp. 585–595, 2020.
- [39] A. Barrau, “Non-linear state error based extended Kalman filters with applications to navigation,” Ph.D. dissertation, Mines Paristech, 2015.
- [40] M. Ghaffari, R. Zhang, M. Zhu, C. E. Lin, T.-Y. Lin, S. Teng, T. Li, T. Liu, and J. Song, “Progress in symmetry preserving robot perception and control through geometry and learning,” *Frontiers in Robotics and AI*, vol. 9, 2022. [Online]. Available: <https://www.frontiersin.org/articles/10.3389/frobt.2022.969380>
- [41] C. Campos, R. Elvira, J. J. G. Rodríguez, J. M. Montiel, and J. D. Tardós, “Orb-slam3: An accurate open-source library for visual, visual-inertial, and multimap slam,” *IEEE Transactions on Robotics*, vol. 37, no. 6, pp. 1874–1890, 2021.
- [42] J. J. Park, S. Lee, and B. Kuipers, “Discrete-time dynamic modeling and calibration of differential-drive mobile robots with friction,” in *Proceedings of the IEEE International Conference on Robotics and Automation*. IEEE, 2017, pp. 6510–6517.
- [43] D. Wisth, M. Camurri, and M. Fallon, “Preintegrated velocity bias estimation to overcome contact nonlinearities in legged robot odometry,” in *Proceedings of the IEEE International Conference on Robotics and Automation*. IEEE, 2020, pp. 392–398.